Sound wave channelling in near-critical sulfur hexafluoride (SF_6)

Author(s):
Schlamp, Stefan; Rösgen, Thomas

Publication Date:
2004

Permanent Link:

https://doi.org/10.3929/ethz-a-005706926 →

Sound wave channelling in near-critical sulfur hexafluoride (SF_6)

Stefan Schlamp[a] and Thomas Rösgen
ETH Zürich, Institute of Fluid Dynamics, Switzerland

(Received 13 February 2003; revised 10 December 2003; accepted 23 December 2003)

Strong density and speed of sound gradients exist in fluids near their liquid-vapor critical point under gravity. The speed of sound has an increasingly sharp minimum and acoustic waves are channelled within a layer of fluid. Geometrical acoustic calculations are presented for different isothermal fluid columns of sulfur hexafluoride (SF_6) under gravity using a semiempirical crossover equation of state. More than 40% of the emitted acoustic energy is channelled within a 20 mm high duct at 1 mK above the critical temperature. It is shown how, by changes in temperature, frequency, and gravitational strength, the governing length scales (wavelength, radius of ray curvature, and correlation length of the critical density fluctuations) can be varied. Near-critical fluids allow table-top sound channel experiments. © *2004 Acoustical Society of America.*
[DOI: 10.1121/1.1648319]

PACS numbers: 43.20.Dk, 43.20.Mv, 64.60Fr [RR] Pages: 980–985

NOMENCLATURE

Fluid and equation of state parameters

a	speed of sound
A	Helmholtz free energy
$\tilde{A}_j$	parameters for analytic background of Helmholtz free energy ($j=0,...,4$); see Table I
c, c_ρ, c_t, d_1	scaling field coefficients; see Table I
C_v, C_p	specific heats at constant volume and pressure
M	densitylike order parameter; defined by Eq. (6)
p	pressure
t	temperaturelike order parameter; defined by Eq. (5)
T	Temperature
u	crossover parameter; see Table I
u^*	universal fixed-point coupling constant; see Table I
V	volume
Y	crossover function; defined by Eqs. (9) and (10)
T_c, ρ_c, p_c	temperature, density, and pressure at liquid-vapor critical point; see Table I
χ	susceptibility
κ	proportional to fluctuation-induced portion of the inverse correlation length; defined by Eq. (10)
μ	specific chemical potential
ξ	correlation length of critical density fluctuations
ρ	density
Λ	dimensionless cutoff wave number; see Table I
α_c, ν_c, γ_c, η_c	critical exponents; see Table I
a_05, a_06, a_14, a_22	parameters from classical mean-field theory; see Table I
Δ_S, Δ_A	critical exponents of symmetric and asymmetric correction terms; see Table I
$\tilde{\mu}_j$	parameters for analytic background of chemical potential ($j=0,...,4$); see Table I
$\mathcal{T}$, $\mathcal{D}$, $\mathcal{U}$, $\mathcal{V}$, $\mathcal{K}$	rescaling functions, defined by Eq. (8)

Acoustics parameters

f	frequency of acoustic source
g	constant of gravity ($=9.81$ m/s^2)
h	height of duct ($=20$ mm)
$\hat{\mathbf{n}}$	unit vector perpendicular to wavefront
R, R^+, R^-	range of loop, range of upper/lower cycle section
r	radius of curvature of rays
$r_{\min}$	defined by Eq. (16)
$\mathbf{s}=(s_x,s_y,s_z)$	wave slowness vector ($=\hat{\mathbf{n}}/a$ for fluid at rest)
t	time
$\mathbf{x}=(x,y,z)$	coordinate vector
Y	crossover function; defined by Eqs. (9) and (10)
η	waveguide efficiency
λ	wavelength of acoustic waves ($=a/f$)
τ, τ^+, τ^-	propagation times associated with R, R^+, and R^-

[a]Author to whom correspondence should be addressed; Electronic mail: schlamp@ifd.mavt.ethz.ch

I. INTRODUCTION

Bending of waves occurs when the gradient of the propagation speed in the direction perpendicular to the direction of propagation is nonzero. In this case, the wave bends in the direction of smaller propagation speeds. This is observed at interfaces as well as for smooth gradients. Consider, for example, optical lenses made from glass of smoothly varying index of refraction or the phenomenon of sound shadows after big explosions.[1] Assuming that the speed of wave propagation only varies in one direction and that it has a local minimum, rays can be channelled within a finite material layer. If no such minimum exists, but if the propagation speed decreases towards an interface (e.g., water surface) then the waves are reflected at the interface and channelling is possible, where the interface represents one boundary of the wave channel. Wave channelling purely by means of reflection (e.g., in an optical fiber) is also possible. Waveguides involving the reflection from an interface are not considered as wave channelling devices for the purpose of this work. Interest in sound wave channelling has mostly focused on underwater sound propagation in the context of long-range communication,[2–5] submarine detection and detection avoidance, and global temperature sounding.[6] Pedersen *et al.*[7,8] examine a range of sound speed profiles, both generic and from measured data in the Pacific.

Critical phenomena in fluids, i.e., the behavior of fluids in the vicinity of the vapor-liquid critical point, have gained a lot of interest in physics and thermodynamics. Near the critical point, many thermodynamic properties, such as the isothermal compressibility, diverge. At the same time, the correlation length of the density fluctuations, which normally is microscopic, becomes macroscopic, causing the phenomenon of critical opalescence when the correlation length becomes comparable to the wavelength of visible light. Since the isothermal compressibility tends to infinity when approaching the critical point, the fluid collapses under its own weight in the presence of gravity. Very steep density gradients over short vertical distances (10% over 1 mm; also see Fig. 1) result. Along with the density profile goes a variation of the speed of sound. An increasingly sharp minimum is observed near the point where the density equals the critical density as one approaches the critical temperature [Fig. 2(a)].

In the present work, numerical results are presented for SF_6. This choice is motivated by several factors: First, by the availability of a suitable equation of state, second, by the experimentally convenient location of the critical point (see Table I), and last by the availability of SF_6 in good purities due to its applications in the semiconductor industry. Xenon and CO_2 are similarly popular for experiments with near-critical fluids, but adequate equations of state for these fluids are not available to date.

II. SETUP AND PROCEDURE

A. Setup

A duct of height $h=20\,\mathrm{mm}\,(z=-10\ldots+10\,\mathrm{mm})$ is considered, which is filled with near-critical, isothermal, pure sulfur hexafluoride (SF_6). Due to gravity and the large compressibility, a density and consequently a speed of sound profile develops in the duct. By choosing the average density in the duct such that $a(+10\,\mathrm{mm})=a(-10\,\mathrm{mm})$ and by placing the acoustic point source at the sound speed minimum, the waveguide efficiency is maximized. The walls of the test duct are assumed to be perfectly absorbing, i.e., wave reflections are neglected.

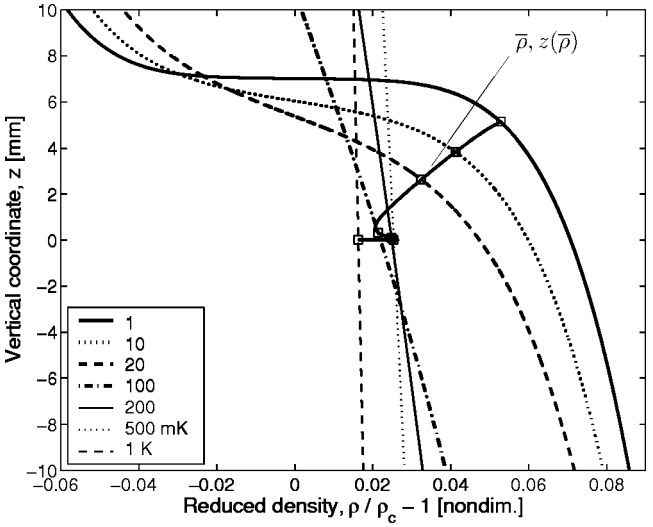

FIG. 1. Density profiles in isothermal fluid columns of near-critical SF_6 under gravity for different temperatures above T_c. The average density is chosen such that $a(-10\,\mathrm{mm})=a(+10\,\mathrm{mm})$ [see Fig. 2(a)]. The symbols mark the average density in the duct and the location at which it is equal to the local density.

B. Equation of state

Critical phenomena are not captured by analytical equations of state. Wyczalkowska *et al.*[9] propose a semiempirical equation of state for SF_6, which shows the correct singular behavior near the critical point (including the correct critical exponents) and crosses over smoothly to regular thermody-

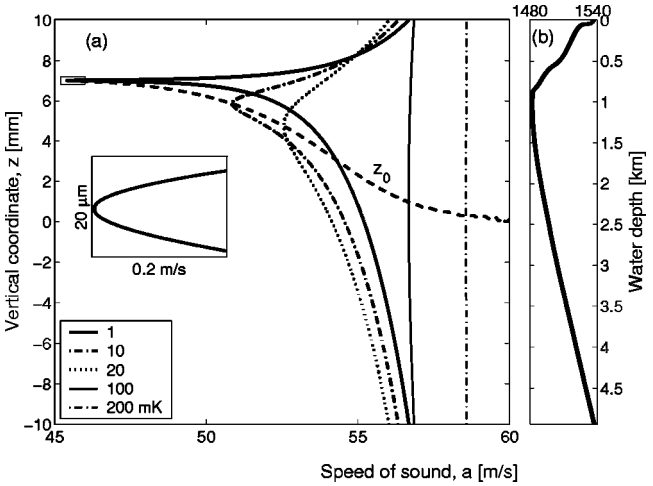

FIG. 2. (a) Left, speed of sound profiles in isothermal fluid columns of near-critical SF_6 under gravity for different temperatures above T_c. The dashed line labeled z_0 connects the sound speed minima. The inset shows a magnification of the minimum for $T-T_c=1\,\mathrm{mK}$ in the range $z=\pm 20\,\mu\mathrm{m}$; (b) right, Sound speed profile in the Pacific ocean after Pedersen *et al.* (Ref. 8). The two panels are drawn such that the relative scales for the speed of sound match (with respect to the sound speed at the panel centers).

TABLE I. Parameters for equation of state (adopted from Wyczalkowska *et al.*[9]). The first two caloric background coefficients only influence the zero of energy and entropy.

Critical point			T_c	318.717	K
			ρ_c	742	kg/m^3
			p_c	3.7545	MPa
Crossover parameters			$\overline{u}$	0.500 43	
			Λ	0.806 21	
Scaling field parameters			c_t	1.737 90	
			c_ρ	2.400 61	
			c	−0.069 04	
			d_1	−0.792 71	
Classical parameters			a_{05}	0.168 38	
			a_{06}	0.732 51	
			a_{14}	0.550 23	
			a_{22}	1.226 24	
Critical exponents					
ν_c	α_c	γ_c	Δ_S	Δ_A	u^*
0.630	0.110	1.239	0.51	1.32	0.472
Equation of state and caloric background parameters					
j	0	1	2	3	4
$\tilde{A}_j$	−1	−6.064 33	7.715 01	−3.085 01	6.700 90
$\tilde{\mu}_0$	N/A	N/A	−34.212 10	0.373 34	−59.998 10

namic behavior away from the critical point. Results as they are relevant for the present work are summarized here. For a more detailed derivation, the reader is referred to Ref. 9.

Nondimensionalize the density, temperature, chemical potential μ, Helmholtz free energy A, the heat capacities C_p and C_v, and the susceptibility χ by

$$\tilde{\rho}=\rho/\rho_c, \quad \tilde{T}=-T_c/T,$$
$$\tilde{\mu}=\frac{\rho_c T_c}{p_c}\frac{\mu}{T}, \quad \tilde{A}=\frac{T_c}{p_c}\frac{A}{VT}, \tag{1}$$
$$\tilde{C}_{p,v}=\frac{T_c}{p_c}\frac{C_{p,v}}{V}, \quad \tilde{\chi}=\left.\frac{\partial\tilde{\rho}}{\partial\tilde{\mu}}\right|_T.$$

The Helmholtz free energy and the chemical potential are expressed in terms of an analytic background $\tilde{A}_0$ and $\tilde{\mu}_0$, respectively, and a critical part $\Delta\tilde{A}$ and $\Delta\tilde{\mu}$, respectively,

$$\tilde{A}=\Delta\tilde{A}+\tilde{\rho}\tilde{\mu}_0(\Delta\tilde{T})+\underbrace{\sum_{j=0}^{4}\tilde{A}_j(\Delta\tilde{T})^j}_{\tilde{A}_0(\Delta\tilde{T})}, \tag{2}$$

$$\tilde{\mu}=\underbrace{\left.\frac{\partial\Delta\tilde{A}}{\partial\Delta\tilde{\rho}}\right|_{\Delta\tilde{T}}}_{\Delta\tilde{\mu}}+\underbrace{\sum_{j=0}^{4}\tilde{\mu}_j(\Delta\tilde{T})^j}_{\tilde{\mu}_0(\Delta\tilde{T})}, \tag{3}$$

where $\Delta\tilde{\rho}=\tilde{\rho}-1$ and $\Delta\tilde{T}=\tilde{T}+1$. The constants $\tilde{A}_j$ and $\tilde{\mu}_j$ are obtained from a fit to experimental data. They are given in Table I, which also contains the parameters which will be introduced subsequently.

The critical part of the Helmholtz free energy is given by

$$\Delta\tilde{A}=\Delta\tilde{A}_x-c\left.\frac{\partial\Delta\tilde{A}_x}{\partial M}\right|_t\left.\frac{\partial\Delta\tilde{A}_x}{\partial t}\right|_M, \tag{4}$$

where

$$t=c_t\Delta\tilde{T}+c\left.\frac{\partial\Delta\tilde{A}_x}{\partial M}\right|_t, \tag{5}$$

$$M=c_\rho(\Delta\tilde{\rho}-d_1\Delta\tilde{T})+c\left.\frac{\partial\Delta\tilde{A}_x}{\partial t}\right|_M, \tag{6}$$

are temperaturelike and densitylike order parameters and

$$\Delta\tilde{A}_x=\frac{1}{2}tM^2\mathcal{T}\mathcal{D}+\frac{u^*\overline{u}\Lambda}{24}M^4\mathcal{D}^2\mathcal{U}+\frac{1}{60}a_{05}M^5\mathcal{D}^{5/2}\mathcal{V}\mathcal{U}$$
$$+\frac{1}{360}a_{06}M^6\mathcal{D}^3\mathcal{U}^{3/2}+\frac{1}{24}a_{14}tM^4\mathcal{T}\mathcal{D}^2\mathcal{U}^{1/2}$$
$$+\frac{1}{4}a_{22}t^2M^2\mathcal{T}^2\mathcal{D}\mathcal{U}^{-1/2}-\frac{1}{2}t^2\mathcal{K}. \tag{7}$$

$\mathcal{T}$, $\mathcal{D}$, $\mathcal{U}$, $\mathcal{V}$, and $\mathcal{K}$ are rescaling functions defined as

$$\mathcal{T}=Y^{(2\nu_c-1)/\Delta_S}, \quad \mathcal{D}=Y^{-\eta_c\nu_c/\Delta_S}, \quad \mathcal{U}=Y^{\nu_c/\Delta_S},$$
$$\mathcal{V}=Y^{(\Delta_A-\nu_c/2)/\Delta_S}, \quad \mathcal{K}=\frac{\nu}{\alpha_c\overline{u}\Lambda}(Y^{-\alpha_c/\Delta_S}-1). \tag{8}$$

η_c is related to the other critical exponents (see Table I) by $\eta_c=2-\gamma_c/\nu_c$. Y is the crossover function, which is found by solving the coupled algebraic equations

$$1-(1-\overline{u})Y=\overline{u}Y^{\nu_c/\Delta_S}\left(1+\left(\frac{\Lambda}{\kappa}\right)^2\right)^{1/2}, \tag{9}$$

$$\kappa^2=t\mathcal{T}+\frac{u^*\overline{u}\Lambda}{2}M^2\mathcal{D}\mathcal{U}+\frac{1}{6}a_{05}M^3\mathcal{D}^{3/2}\mathcal{V}\mathcal{U}$$
$$+\frac{1}{24}a_{06}M^4\mathcal{D}^2\mathcal{U}^{3/2}+\frac{1}{2}a_{14}tM^2\mathcal{T}\mathcal{D}\mathcal{U}^{1/2}$$
$$+\frac{1}{2}a_{22}t^2\mathcal{T}^2\mathcal{U}^{-1/2}. \tag{10}$$

The pressure and the speed of sound are related to the chemical potential and the Helmholtz free energy by

$$\tilde{p}=\tilde{\rho}\tilde{\mu}-\tilde{A}, \tag{11}$$

$$\tilde{a}=\left(\frac{\tilde{\rho}}{\tilde{\chi}}\frac{\tilde{C}_p}{\tilde{C}_v}\right)^{1/2}, \tag{12}$$

with

$$\frac{\tilde{C}_v}{\tilde{T}^2}=-\frac{d^2\tilde{A}_0(\tilde{T})}{d\tilde{T}^2}-\tilde{\rho}\frac{d^2\tilde{\mu}_0(\tilde{T})}{d\tilde{T}^2}-\left.\frac{\partial^2\Delta\tilde{A}}{\partial\Delta\tilde{T}^2}\right|_{\Delta\tilde{\rho}}, \tag{13}$$

$$\tilde{C}_p=\tilde{C}_v+\frac{\tilde{\chi}}{\tilde{\rho}^2}\left(\tilde{p}-\tilde{T}\left.\frac{\partial\tilde{p}}{\partial\tilde{T}}\right|_{\tilde{\rho}}\right)^2. \tag{14}$$

For the purpose of this work, only the relationships $p(\rho,T)$ and $a(\rho,T)$ are used. The relationship $\rho(p,T)$ is implemented by iteratively solving $p(\rho,T)$.

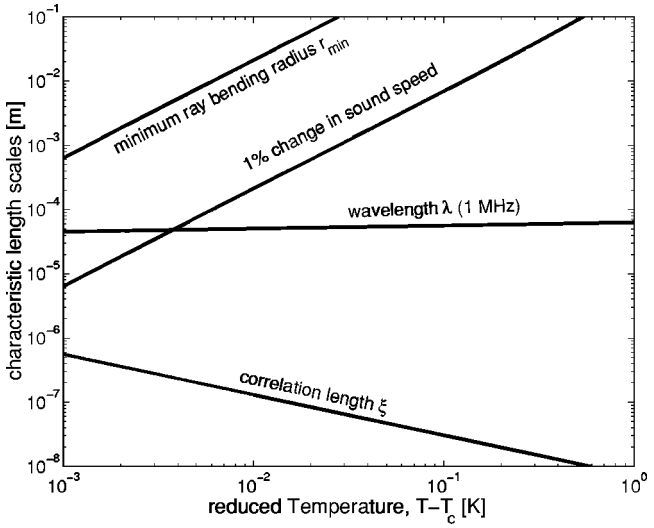

FIG. 3. Relevant characteristic length scales for an acoustic source with $f=1$ MHz located in an isothermal fluid column (height $h=20$ mm) of near-critical SF_6 at the sound speed minimum. The acoustic wavelength is at least two orders of magnitude larger than the correlation length of the critical fluctuations and at least one order smaller than the minimum ray bending radius. For reference, the minimum vertical distance over which the speed of sound changes by 1% is shown.

C. Geometrical acoustics

Geometrical acoustics assumes that the radius of curvature of rays is much larger than the wavelength and that the amplitude does not change significantly over the same length scale. These assumptions simplify the general solution of the wave equation. For rays in an inhomogeneous medium at rest, one finds[1]

$$\frac{d\mathbf{s}}{dt}=-\frac{1}{a}\nabla a \quad \text{and} \quad \frac{d\mathbf{x}}{dt}=a^2\mathbf{s}, \tag{15}$$

where $\mathbf{s}=(s_x,s_y,s_z)=\hat{\mathbf{n}}/a$ denotes the wave slowness and a is the local speed of sound.

For a given temperature, the smallest possible radius of curvature of a ray is

$$r_{\min}=\min_{|z|\leqslant 10\ \mathrm{mm}}\left\{\frac{a}{da/dz}\right\}, \tag{16}$$

which is observed for a ray perpendicular to the sound speed gradient. In order for the geometrical limit to be applicable, this length scale has to be much larger than the wavelength of the acoustic waves, $r_{\min}\gg\lambda$. The correlation length of the critical density fluctuations on the critical isochore is[9]

$$\xi=\xi_0^+\left|\frac{T}{T_c}-1\right|^{-\nu_c}, \quad \rho=\rho_c, \quad T>T_c \tag{17}$$

with $\xi_0^+=0.19$ nm and $\nu_c=0.630$. This neglects the limiting effect of gravity. When $\lambda\gg\xi$, then the diffraction of the acoustic waves at the critical fluctuations is negligible. The wavelength can be adjusted by varying the driving frequency of the transducer. Figure 3 shows the characteristic length scales for the case $f=1$ MHz. The wavelength satisfies both conditions, namely $\lambda\gg\xi$ and $\lambda\ll r_{\min}$. Mueller *et al.*[10] and examine ultrasonic attenuation in near-critical xenon. Kogan *et al.*[11] present experimental results on critical attenuation and dispersion in He-3 and He-4. No such data exists for sulfur hexafluoride. Onuki[12] reviews some theoretical concepts of critical sound attenuation. It is assumed that attenuation does not invalidate the assumption of ray acoustics.

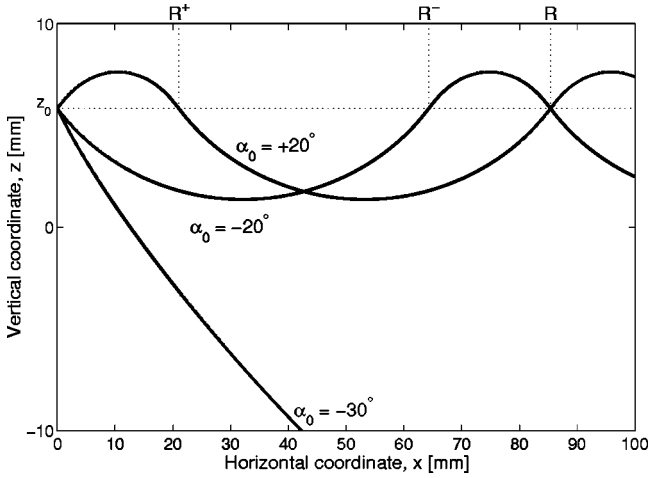

FIG. 4. Rays emanating with different initial ray angles from an acoustic point source located at the sound speed minimum in isothermal, near-critical SF_6 at $T-T_c=10$ mK under gravity. Reflections from the duct boundaries are not considered.

D. Numerical integration of the ray equations

Density profiles are calculated iteratively for a range of temperatures. Initially, they span a range of z values, which is much larger than the duct height. A uniform density is used as starting value, from which a vertical pressure distribution is obtained by integration in z direction. An improved density profile then follows from the equation of state. This procedure converges after a few iterations. The sound speeds corresponding to the density profile are calculated subsequently from the equation of state. Finally, a 20 mm section of the profile is extracted, for which $a(-10\,\mathrm{mm})=a(+10\,\mathrm{mm})$. Integrating the densities over this section yields the average density $\overline{\rho}$.

Given speed of sound profiles, the ray equations (15) are integrated numerically using a fifth order Runge–Kutta scheme (Dormand–Prince pair).[13] Initial conditions

$$\mathbf{x_0}=(0,0,z_0) \quad \text{and} \quad \mathbf{s_0}=(\cos\alpha_0/a(z_0),0,\sin\alpha_0/a(z_0)) \tag{18}$$

are used to calculate rays originating at different initial ray angles α_0 from a source at z_0, the location of the sound speed minimum. Figure 4 shows a few representative rays for the case $T-T_c=10$ mK.

III. RESULTS

Figure 1 depicts the calculated density profiles for isothermal sulfur hexafluoride under gravity ($g=9.81\,\mathrm{m/s^2}$). For temperatures away from the critical point, the density varies linearly with the vertical coordinate. When the temperature approaches T_c, the range of densities increases and the profile becomes nonlinear. The total density variation over 20 mm increases from 0.24% for $T-T_c=1$ K to 14.4% for $T-T_c=1$ mK, where an increasing fraction of the

total density variation is limited to an increasingly narrow region. For $T-T_c=1$ mK, for example, the density varies by 10% over 1 mm.

Given a temperature, the vertical shift of the density profiles in Fig. 1 is controlled by the average density $\overline{\rho}$ in the duct. It is found from the condition that $a(-10\,\mathrm{mm})=a(+10\,\mathrm{mm})$. The symbols in Fig. 1 mark the results for $\overline{\rho}$ and the location where $\overline{\rho}=\rho$. In an experiment one would fill the test section with the appropriate average density and then equilibrate the duct at the desired temperature, which can take hours or even days, depending on the temperature and the size of the fluid volume.

The sound speed profiles, which provide the vertical reference for the density profiles, are shown in Fig. 2(a) for a selection of temperatures. The sound speeds generally increase with increasing temperature and an increasingly sharp minimum develops as one approaches the critical temperature from above. As required, the speeds of sound at the top and bottom of the duct are identical. Due to the global properties of the sound speed profile (no local maxima), this places the local sound speed minimum within the duct. The dashed line connects the location of the sound speed minima. Since the acoustic point source is located at the sound speed minimum, its location is used as one of the initial conditions for Eqs. (15) and is therefore denoted by z_0. The sound speed profiles are not symmetric with respect to the minima, which are thus off center. For $T-T_c=1$ mK, for example, the sound speed minimum is located at $z=+7$ mm. For larger reduced temperatures, the location of the minimum approaches the center line. The inset in Fig. 2(a) shows a magnification of the sound speed minimum for $T-T_c=1$ mK. The minimum is not a cusp, but smooth and numerically well resolved. Figure 2(b) shows the speed of sound variation vs depth below MSL at a point in the Pacific Ocean for comparison.[8] The horizontal scales and panel sizes in Figs. 2(a) and (b) are chosen such that the relative variation of the speed of sound is preserved. The total variation is approximately 4% over 4700 m. The same variation is achieved over 20 mm in near-critical SF_6 at a temperature of $T-T_c=31$ mK.

Figure 3 shows plots of the relevant length scales. The acoustic wavelength (assuming a frequency of 1 MHz) increases by 40% between $T-T_c=1$ K and 1 mK. The correlation length of the critical density fluctuation ξ and the minimum ray bending radius $r_{\min}$ depend more strongly on the temperature. ξ increases by almost two orders of magnitude as one approaches T_c. Over the same range of temperatures, $r_{\min}$ decreases by more than six orders of magnitude. For all temperatures under consideration, the requirements for geometrical acoustics to be applicable, $\xi \ll \lambda$ and $r_{\min} \gg \lambda$, is satisfied. Also plotted in Fig. 3 is the minimum vertical distance over which the speed of sound varies by 1%.

Some example results of the numerically integrated ray equations are shown in Fig. 4. The temperature is $T-T_c=10$ mK. For initial angles $\alpha_{0,\min} \leqslant \alpha_0 \leqslant \alpha_{0,\max}$, rays can propagate within $|z| \leqslant 10$ mm. Because $a(10\,\mathrm{mm})=a(-10\,\mathrm{mm})$, $\alpha_{0,\max}=-\alpha_{0,\min}$ by construction. Rays with $|\alpha_0|>\alpha_{0,\max}$ hit the upper or lower duct boundary as shown in Fig. 4 for the ray with $\alpha_0=-30°$. For channelled rays,

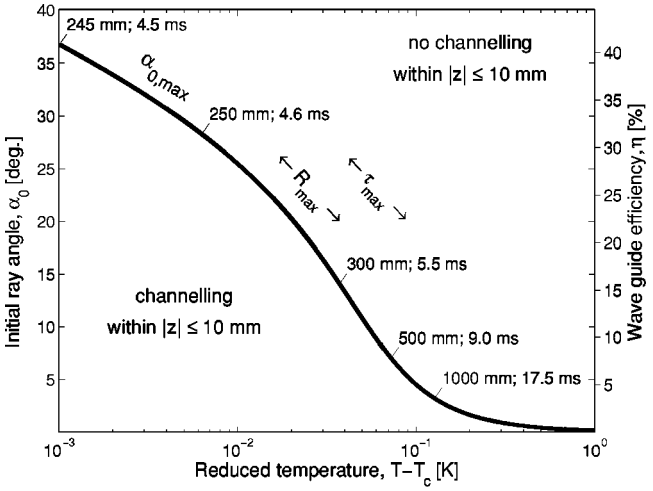

FIG. 5. Maximum initial ray angle $\alpha_{0,\max}=-\alpha_{0,\min}$ for ray channelling to occur in 20 mm of isothermal, near-critical SF_6 under gravity. The numerical values represent ranges and corresponding loop times for $\alpha_0=\alpha_{0,\max}$. The scale on the right shows the corresponding channelling efficiency.

the length of a ray loop is referred to as range $R=R^+ +R^-$,[8] where R^+ and R^- are the ranges of the ray loop above and below z_0, respectively. The propagation times over one loop is denoted by τ. Like the sound speed profiles, the waves are not symmetric with respect to $z=z_0$. By construction, however, the range is independent of the sign of α_0.

Snell's law applied to the current example is[7]

$$\cos \alpha_{0,\max}=\frac{a_{\min}}{a_{\max}}=\frac{a(z_0)}{a(10\ \mathrm{mm})}. \tag{19}$$

The maximum initial ray angles as function of the temperature are plotted in Fig. 5. The fraction of acoustic energy channelled within the duct out of the total emitted energy is the waveguide efficiency η. It is

$$\eta=\frac{2\alpha_{0,\max}}{180°}. \tag{20}$$

The scale for the waveguide efficiency is plotted in the secondary vertical axis on the right of Fig. 5. $\alpha_{0,\max}$ does not seem to level off as one approaches T_c. At a reduced temperature of 1 mK, $\alpha_{0,\max}=36.8°$. This value drops to 25.5° and 4.55° for $T-T_c=10$ mK and 100 mK, respectively. Corresponding to $\alpha_{0,\max}(T)$ is a range $R_{\max}$ and a run time of the acoustic waves over one loop $\tau_{\max}$. Some typical values are given in Fig. 5. Initially the range $R_{\max}$ increases very slowly with increasing reduced temperature. It only doubles (from 245 mm to 500 mm) over almost two orders of magnitude in $T-T_c$ (1 mK to 70 mK), but doubles again between 70 mK and 110 mK.

IV. CONCLUSIONS

The effect of dispersion, which is observed near the critical point,[14–18] has been neglected in the present analysis. The definition of the speed of sound is the limit for zero frequency, which is the speed of sound given by the equation of state. The sound speed profiles for higher frequencies might therefore be different from those shown in Fig. 2. Dy-

TABLE II. The three characteristic length scales (wavelength λ, radius of curvature r, and correlation length ξ) are influenced by the reduced temperature $T-T_c$, the frequency f, and the level of gravity g.

			Wavelength λ	Radius of curvature r	Correlation length ξ
Reduced temperature	$T-T_c$	↑	↑	↑	↓
Frequency	f	↑	↓	?	—
Gravity	g	↑	—	↑	↑

namic critical phenomena are an active area of research and an equation of state providing the speed of sound as function of the thermodynamic variables as well as frequency is not yet available. Likewise, and for the same reason, attenuation has not been considered. The results presented should therefore only be taken as qualitative rather than quantitative. The form of the variations in density and the sound speed along isotherms near the critical point is universal. Other fluids will show the same qualitative behavior. Intramolecular vibrations strongly influence the dispersion relationship such that the speed of sound profiles at a given frequency is fluid dependant.

From Fig. 3 one sees that the three characteristic length scales (wavelength, correlation length, and ray bending radius) become comparable for even smaller reduced temperatures. Interactions between acoustic waves and the critical density fluctuation become significant for $\lambda/\xi=\mathcal{O}(1)$. A smooth transition away from geometrical acoustics can be observed for $r/\lambda=\mathcal{O}(1)$. The length scales can be controlled by the temperature, gravity, and frequency. These effects are summarized qualitatively in Table II. Increasing the temperature, for example, and leaving all other parameters unchanged results (a) in a larger wavelength, because the speed of sound increases with increasing temperature, (b) in a larger radius of curvature through smaller speed of sound gradients, and (c) in a reduced correlation length by being further away from the critical point. The frequency, on the other hand, primarily only impacts the wavelength. Its influence on r by means of dispersion (frequency-dependent sound speed profiles) is not clear. The formation of the density gradients is driven by gravity. In a reduced-gravity environment, these profiles are more uniform and the radius of curvature of the rays is thus larger. Furthermore, very close to the critical point gravity limits the correlation length to approximately 2 μm on earth,[19] but much larger values can be achieved in low-g experiments.

The combination of the two areas of research, wave channelling and critical phenomena, makes it possible to study the former using table-top facilities. Acoustics, on the other hand, can be used to study critical phenomena. While not discussed here, it can be shown that caustics exist for the sound speed profiles shown in Fig. 2. Acoustics could thus be used to introduce local energy disturbances into near-critical fluids. Another application is to use acoustic wave propagation to study the statistics of the critical density and sound speed fluctuations, e.g., as outlined by Ostashev for fluids with random inhomogeneities.[20] Analogous to other tomographic techniques, an experimental setup with several ultrasonic transducers and receivers could yield the sound speed profile within a test section by means of an appropriate reconstruction algorithm.

[1] A. D. Pierce, *Acoustics—An Introduction to Its Physical Principles and Applications* (McGraw-Hill, New York, 1981).
[2] A. G. Bessios and F. M. Caimi, "High-rate wireless data communications: An underwater acoustic communications framework at the physical layer," Math. Problems Eng. **2**, 449–485 (1996).
[3] D. N. Dutt, "Ray transmission in coastal sea using nonlinear velocity profiles," J. Sound Vib. **157**, 538–544 (1992).
[4] D. E. Weston and P. B. Rowlands, "Guided acoustic waves in the ocean," Rep. Prog. Phys. **42**, 347–387 (1979).
[5] W. H. Munk, "Sound channel in an exponentially stratified ocean, with application to SOFAR," J. Acoust. Soc. Am. **55**, 220–226 (1974).
[6] J. A. Schröder, E. R. Westwater, P. T. May, and L. M. McMillin, "Prospects for temperature sounding with satellite and ground-based RASS measurements," J. Atmos. Ocean. Technol. **8**, 506–513 (1991).
[7] M. A. Pedersen, "Ray theory applied to a wide class of velocity functions," J. Acoust. Soc. Am. **43**, 619–634 (1968).
[8] M. A. Pedersen and D. White, "Ray theory for sources and receivers on an axis of minimum velocity," J. Acoust. Soc. Am. **48**, 1219–1248 (1970).
[9] A. K. Wyczalkowska and J. V. Sengers, "Thermodynamic properties of sulfur hexafluoride in the critical region," J. Chem. Phys. **111**, 1551–1560 (1999).
[10] P. E. Mueller, R. C. Williams, D. Eden, and C. W. Garland, "Ultrasonic attenuation and dispersion in xenon near its critical point," Phys. Rev. A **6**, 2272 (1972).
[11] A. B. Kogan and H. Meyer, "Sound propagation in He-3 and He-4 above the liquid-vapor critical point," J. Low Temp. Phys. **110**, 899–918 (1998).
[12] A. Onuki, "Dynamic equations and bulk viscosity near the gas-liquid critical point," Phys. Rev. E **55**, 403–420 (1997).
[13] J. R. Dormand and P. J. Prince, "A family of embedded Runge–Kutta formulae," J. Comput. Appl. Math. **6**, 19–26 (1980).
[14] H. Z. Cummins and H. L. Swinney, "Dispersion of the velocity of sound in xenon in the critical region," Phys. Rev. Lett. **25**, 1165–1169 (1970).
[15] D. Eden, C. W. Garland, and J. Thoen, "Sound absorption and dispersion along the critical isochore in xenon," Phys. Rev. Lett. **28**, 726–729 (1972).
[16] J. Thoen and C. W. Garland, "Sound absorption and dispersion as a function of density near the critical point of xenon," Phys. Rev. A **10**, 1311–1327 (1974).
[17] R. Span, E. W. Lemmon, R. T. Jacobsen, W. Wagner, and A. Yokozeki, "A reference equation of state for the thermodynamic properties of nitrogen for temperatures from 63.151 to 1000 K and pressures to 2200 MPa," J. Phys. Chem. Ref. Data **29**, 1361–1433 (2000).
[18] M. F. C. Gomez and J. P. M. Trusler, "The speed of sound in nitrogen at temperatures between $T=250$ K and $T=350$ K and at pressures up to 30 MPa," J. Chem. Thermodyn. **30**, 527–534 (1998).
[19] M. Moldover, J. Sengers, R. Gammon, and R. Hocken, "Gravity effects in fluids near the gas-liquid critical point," Rev. Mod. Phys. **51**, 79–99 (1979).
[20] V. E. Ostashev, "Sound-propagation and scattering in media with random inhomogeneities of sound speed, density and medium velocity," Waves Random Media **4**, 403–428 (1994).